TÜBİTAK

Turkish Journal of Chemistry

http://journals.tubitak.gov.tr/chem/

Research Article

Turk J Chem
(2013) 37: 344 – 357

doi:10.3906/kim-1206-31

Spectral, electrochemical, luminescence, and dye-sensitized solar cell studies of mono and d-f hetero binuclear cryptates

Arunachalam VIJAYARAJ,[1] Raju PRABU,[1] Ranganathan SURESH,[1] Subbaiah MANOHARAN,[2] Sambandan ANANDAN,[2] Vengidusamy NARAYANAN[1,*]

[1]Department of Inorganic Chemistry, School of Chemical Sciences, University of Madras, Guindy Maraimalai Campus, Chennai, India

[2]Department of Chemistry, National Institute of Technology, Trichy, India

Received: 15.06.2012 • **Accepted:** 08.02.2013 • **Published Online:** 10.06.2013 • **Printed:** 08.07.2013

Abstract: Mono and hetero binuclear cryptates, $[Gd(III)ML]^+$ [M = VO(IV), Co(II), Ni(II), Cu(II)], were synthesized by a 2-step method. The ligand L represents the deprotonated anionic cryptate obtained by the 2+3 condensation of tris-(2-aminoethyl)amine with 2,6-diformyl-4-nitrophenol. The complexes were characterized by elemental analysis, spectral, magnetic, and electrochemical studies. Fluorescence of Gd(III) ion in the cavity was quenched by the encapsulated Cu(II) and Ni(II) ions. $[GdCoL(NO_3)]^+$ cryptate had a high lifetime value compared to other cryptates. The cyclic voltammogram showed that the reduction potential values of [Gd(M)L] M = VO(IV), Co(II), Ni(II), and Cu(II) complexes were in the following order: Cu(II) > Ni(II) > Co(II) > VO(IV). The efficiency (η) of the cryptate based dye-sensitized solar cell (DSSC) increases in the following order: $[GdVOL(NO_3)]^+ < [GdCoL(NO_3)]^+ < [GdCuL(NO_3)]^+ < [GdHL] < [GdNiL(NO_3)]^+$.

Key words: Gadolinium, binuclear complexes, electrochemistry, lifetime decay, DSSC

1. Introduction

In recent years, the growing worldwide demands for energy along with the increasing concerns over global warming have stimulated interest in seeking renewable energy sources. Dye-sensitized solar cells (DSSCs), due to their relatively high efficiency, simple fabrication process, and low-cost production, are potential alternatives to conventional silicon-based photovoltaic devices for the direct conversion of electrical energy.[1–5]

The photosensitizer was one of the key elements for high power conversion efficiencies. DSSC based on Ru-complex dye, cis-dithiocyanato-4,4'-dicarboxy-2,2'-bipyridyl ruthenium(II) complex (N3 dye), can produce high photoelectric conversion efficiency. Several groups have developed new sensitizers and obtained good efficiencies.[6] A typical DSSC comprises a dye-sensitized nano crystalline TiO_2 interpenetrated by a hole-transporting material such as a liquid electrolyte (I^-/I_3^-) redox couple.[7] Absorption of light by the sensitizer creates a high-energy state that can inject the excited electron into the conduction band of TiO_2 and the oxidized dye is regenerated by the redox couple. In this work, an inorganic complex based on Gd(III) was synthesized and used as sensitizer. The relatively low fill factor and efficiency could probably be attributed to the different chemical structure of different metal coordination.

*Correspondence: vnnara@yahoo.co.in

The lanthanide(III) ions are valuable for the development of technological applications such as the selective extraction of metals, NMR image-contrast agents, magnetic resonance imaging agents, fluoroimmuno assay, luminescence labels, and diagnostic agents.[8] In addition, they can also be used as catalysts for RNA cleavage.[9,10] Many lanthanide(III) complexes are able to exhibit fluorescence in the solid state, but their fluorescence efficiency in aqueous solution is substantially lowered, owing to the coordination of water molecules to the lanthanide atoms.[11] Therefore, it is important to protect the metal as efficiently as possible from coordination of water molecules when preparing lanthanide complexes with strong fluorescence properties in aqueous solution. The cryptand ligands possess spherical cavities and special recognition sites toward metal ions and small molecules. They are able to shield the metal ions from interaction with water molecules. Due to their unique properties compared to analogous mononuclear and homodinuclear complexes, there has been a great deal of recent interest in hetero binuclear complexes.[12]

The cryptates have good thermodynamic stability and kinetic inertness toward metal dissociation. The gadolinium cryptates derived from 2,6-diformyl-4-methylphenol(dfm) and tris(2-aminoethyl)amine (tren) have been reported previously by Nelson[13] and Fenton.[14] Feng et al.[15] and Chen et al.[16] have reported the crystal structure and magnetic properties of lanthanide complexes. Hetero binuclear complexes containing both transition metal and lanthanide ions were rarely reported[17] and studies on these complexes were mostly concentrated on magnetic properties of the macrocyclic complexes.[18] Chen et al.[19] first reported d-f hetero binuclear cryptate with the formula [DyCu(L-3H) (DMF)] $(ClO_4)_2$. MeCN] and [GdNi(L^1-3H)]$^+$ $(ClO_4)_2$ as well as the magnetic properties of the Ni(II) derivative. For the first time herein we report dye-sensitized solar cell, fluorescence, and lifetime measurement studies for hetero binuclear cryptates.

Inspired by the wide applications of hetero binuclear cryptates, we successfully synthesized 4 hetero binuclear cryptates [GdML]$^+$ (ClO_4) [M = VO(IV), Co(II), Ni(II), Cu(II)] along with the mononuclear Gd(III) complex and studied the electrochemical behavior. Further, the feasibility of enhancing solar cell performance, fluorescence, and lifetime measurement with hetero binuclear cryptate was investigated.

2. Experimental

2.1. Solvent and starting material

$Gd(NO_3)_3.5H_2O$ (99.9%) and tris(2-aminoethyl)amine (99.9%) (tren) were purchased from Aldrich and 2,6-diformyl-4-nitrophenol (dnp)[20] was synthesized by following the literature procedure. Their physical constants and spectral data were in agreement with literature values. All starting materials were of reagent grade and the solvents were purified by general methods.

2.2. Analytical and physical measurements

Elemental analysis of the complexes was conducted using a Haereus CHN rapid analyzer. Conductivity of the complexes was measured using an Elico digital conductivity bridge model CM-88 with freshly prepared solution of the complex in DMF. The FTIR spectra were recorded on a PerkinElmer FTIR 8300 series spectrophotometer on KBr disks from 4000 to 400 cm^{-1}. Electronic spectral studies were recorded on a PerkinElmer UV-320 spectrophotometer from 200 to 1100 nm. ESI mass spectra were obtained on a JEOL DX-303 mass spectrometer; the concentrations of the samples were about 1.0 μmol dm^{-3}. The diluted solutions were electrosprayed at a flow rate of 5×10^{-6} dm^{-3} min^{-1} with a needle voltage of +4.5 kV. The mobile phase was an aqueous solution of methanol (v/v, 1:1) and the samples were run in the positive-ion mode. Steady state

fluorescence measurements were obtained using a fluorescence spectrophotometer (Fluoromax 4P, Horiba Jobin Yvon). The concentration of the sample solution was 3×10^{-5} M in DMF medium. The fluorescence decay curve and lifetime measurements were carried out using a time correlation single-photon counting spectrometer (IBH, model 5000U). The excitation source was 280 nm nano LED (IBH) with a pulse width of <1 ns. The fluorescence emission was monitored at a right angle to the excitation path and photons were detected by a MCP-PMT (Hamamatsu, model R3809U) detector. The data analysis was carried out by the software provided by IBH (DAS-6), which was based on deconvolution techniques using the nonlinear least-squares method.

2.3. General procedure for electrochemical studies

The cyclic voltammetric experiments were performed on a CHI-600A electrochemical analyzer under oxygen-free conditions using a 3-electrode electrochemical cell in which a glassy carbon electrode was the working electrode, Ag-AgCl was the reference electrode, and a platinum wire was the auxiliary electrode. DMF was used as the solvent. Tetra n-butyl ammonium perchlorate (TBAP) was used as the supporting electrolyte. Experiments were performed under a purified nitrogen atmosphere at 25 $\pm$ 0.1 °C. The oxidation potential of the ferrocene/ferrocenium (Fc/Fc^+) couple under the experimental conditions was 470 mV. All the complex concentrations were 1.05×10^{-3} mol dm^{-3} in 0.1 mol dm^{-3} TBAP DMF solutions. The solutions were degraded for ca. 15 min by purging nitrogen gas before applying the voltage. The half-wave potentials, $E_{1/2}$, were calculated approximately from $(E_{pa} + E_{pc})/2$ and the measured errors were ± 2 mV.

2.4. General procedure (A) for dye-sensitized solar cell studies

2.4.1. Fabrication and photovoltaic measurement of dye-sensitized solar cells (DSSCs)

Nanocrystalline TiO_2 films were prepared on the conducting glass support (fluorine doped SnO_2, FTO, sheet resistance 10 $\Omega/\square$).[21] Coating of the TiO_2 surface with the dye was carried out by dipping the electrode (maintained at 80 °C) in a 3×10^{-4} M solution of the gadolinium complexes in DMF for 24 h. The occurrence of color change immediately after immersion of the glass plates confirms the attachment of dye on the semiconductor surface. After the dye adsorption was complete, the electrode was withdrawn from the solution and dried under a stream of argon. The regenerative photo-electrochemical cell was fabricated by sandwiching dye-coated TiO_2 film with a thin platinum-coated conductive glass support,[22] which serves as the counter electrode, while iodine/iodide (0.5 M KI, 0.05 M I_2 and 0.5 M 4-tert-butylpyridine (TBP) dissolved in 2-methoxypropionitrile) was employed as a redox electrolyte. The electrodes were clipped together and illuminated through the TiO_2-sensitized surface. For comparison, a similar cell was fabricated with standard (cis-bis(isothiocyanato)bis(2,2′-bipyridyl-4,4′-dicarboxylato)-ruthenium(II) (N3 dye). In order to examine the device's performance, the current density (J)–voltage (V) characteristics of the fabricated solar cells were measured in the dark and under illumination (LOT solar simulator of intensity 40 mW/cm^2) using an Autolab N_3O_2 potentiostat/galvanostat.

2.4.2. Synthesis of mononuclear Gd(III) complex

An absolute methanol solution (20.0 mL) containing tren (0.149 g, 1.00 mmol) was added dropwise to a stirred mixed solution of (0.246 g, 1.50 mmol) dmp and $Gd(NO_3)_3.5H_2O$ (0.238 g, 0.55 mmol) in 20.0 mL of absolute methanol. After refluxing for 4–5 h, the cotton-like precipitate was filtered while the solution was hot and the

precipitate was discarded. To the filtrate was added 15.0 mL of dry acetonitrile. Evaporating the solution to one-fourth of its original volume at room temperature resulted in the yellowish product [Gd(HL) (NO_3)], which was filtered and washed with methanol and then diethyl ether and air dried. The above reaction is shown in Scheme 1. The complex is air stable and soluble in dimethylsulfoxide and dimethylformamide; moderately soluble in water, acetonitrile, ethanol, and methanol; and slightly soluble in chloroform.

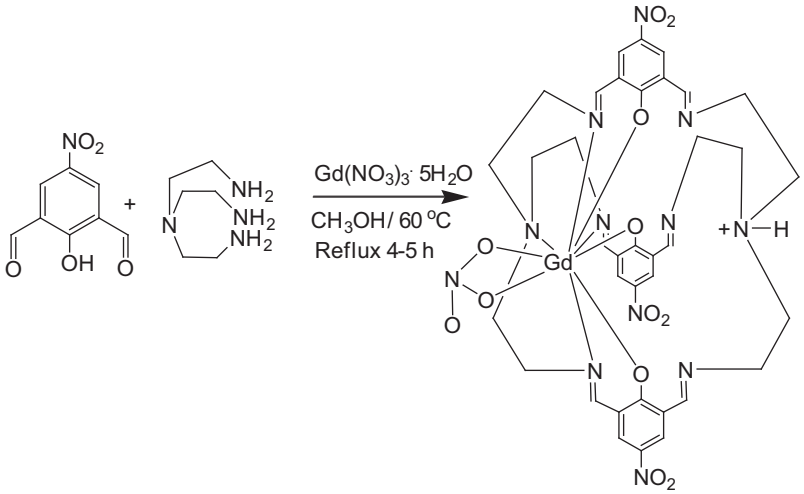

Scheme 1. Schematic diagram for the synthesis of mononuclear [GdLH(NO_3)] complex.

[Gd(HL)(NO_3)]·2H_2O 1

Yellowish solid. Yield: 0.1020 g, (71%). Anal. Calc. for [$C_{36}H_{37}N_{12}O_{12}Gd$] (%): C, 43.81; H, 3.78; N, 17.03. Found: C, 43.50; H, 3.56; N, 16.54%. ESI MS: (m/z) 988.20 [MH^+]. Calcd av. m/z 987.18. Selected IR (KBr, cm^{-1}) 3416 w [ν (OH)]; 1640 s [ν (C=N); 1540 s [ν (C-O)]; 1478 s [ν (N=O)]; 1367 s [$\nu(NO_3^-)$]; 1281 s [$\nu_{asym}(NO_2)$ and 1078 s [$\nu_{sym}(NO_2)$].

2.4.3. Synthesis of binuclear complex

Mononuclear gadolinium(III) cryptate (0.0911 g, 0.1 mmol) was dissolved in methanol (15 cm^3) containing a small amount of DMF (1.0 cm^3). The pH of the solution was adjusted to 7–8 with CaH_2 and filtered. Vanadium perchlorate (0.036 g, 0.1 mmol) was added to the filtrate and the mixture was refluxed for ca. 4 h. The solution was then concentrated until a yellowish green product formed. The complex is soluble in DMF and DMSO and it has low solubility in MeCN and MeOH. Complexes $[GdCoL]^+$, $[GdNiL]^+$, and $[GdCuL]^+$ were synthesized by following the above procedure using $Co(ClO_4)_2.5H_2O$ (0.034 g, 0.1 mmol), $Ni(ClO_4)_2.5H_2O$ (0.035 g, 0.1 mmol), and $Cu(ClO_4)_2.6H_2O$ (0.037 g, 0.1 mmol) instead of $VO(ClO_4)_2.5H_2O$. The above reaction is shown in Scheme 2.

$[GdVOL(NO_3)]^+$ (ClO_4) 2

Yellowish green solid. Yield: 0.0720 g, (55%). Anal. Calc. [$C_{36}H_{36}N_{12}O_{13}VGd$]: C, 41.06; H, 3.45; N, 15.96. Found: C, 40.55; H, 3.25; N, 15.57%. ESI MS: (m/z) 1054.19 [MH^+], Calcd av. m/z 1053.10. Selected IR (KBr, cm^{-1}) 1645 s [ν(C=N)]; 1544 s [ν(C–O)]; 1299 [$\nu(NO_3^-$]; 1055 [$\nu(ClO_4)$]; 1085 s [ν(VO)]. Λm (DMF, 298 K): 136 S cm^2 mol^{-1}.

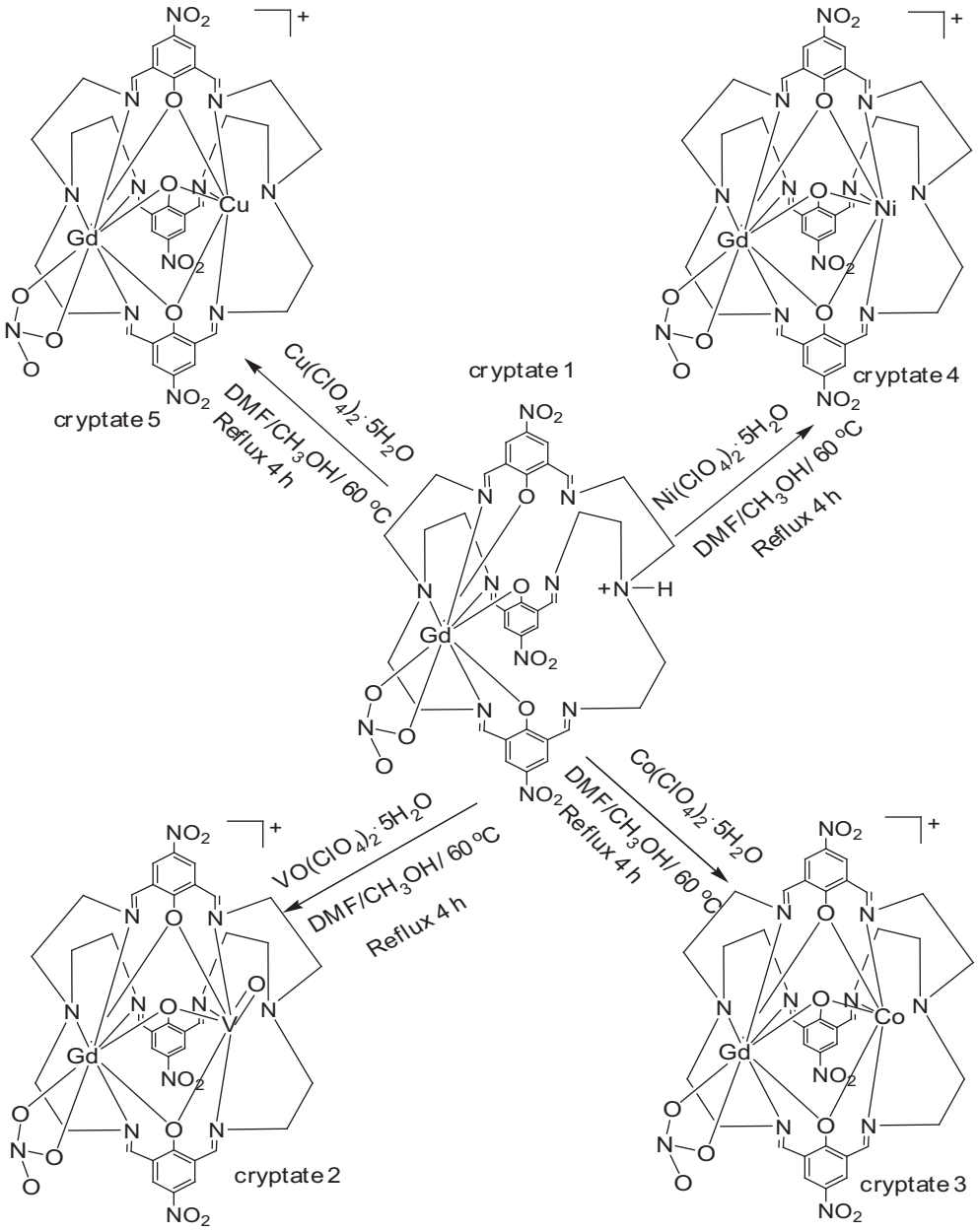

Scheme 2. Schematic diagram for the synthesis of binuclear complexes.

$[GdCoL(NO_3)]^+$ (ClO_4) 3

Yellowish brown solid. Yield: 0.0800 g, (61%). Anal. Calc. [$C_{36}H_{36}N_{12}O_{12}CoGd$]: C, 41.38; H, 3.45; N, 16.09. Found: C, 41.04; H, 3.28; N, 15.64%. ESI MS: (m/z) 1046.19 [MH^+]. Calcd av. m/z 1045.10. Selected IR (KBr, cm^{-1}) 1642 s [ν(C=N)]; 1528 s [ν(C–O)]; 1231 [$\nu(NO_3^-$] 1070 s [$\nu(ClO_4)$]; 615 m [$\nu(ClO_4\Lambda m$ (DMF, 298 K): 134 S cm^2 mol^{-1}.

$[GdNiL(NO_3)]^+$ (ClO_4) 4

Yellowish green solid. Yield: 0.0790 g, (59%). Anal. Calc. [$C_{36}H_{36}N_{12}O_{12}NiGd$]: C, 41.39; H, 3.85; N, 16.84%. Found: C, 41.11; H, 3.46; N, 16.56%. ESI MS: (m/z) 1045.19 [MH^+], Calcd av. m/z 1046.10. Selected

IR (KBr, cm^{-1}) 1635 s [ν(C=N)]; 1531 s [ν(C–O)]; 1125 [$\nu(NO_3^-$]; 1085 s [$\nu(ClO_4)$]; 605 m [ν(M-O)]; Λm (DMF, 298 K): 132 S cm^2 mol^{-1}.

[GdCuL(NO_3)]$^+$ (ClO_4) 5

Yellowish green solid. Yield: 0.0820 g, (65%). Anal. Calc. [$C_{36}H_{36}N_{12}O_{12}CuGd$]: C, 41.20; H, 3.45; N, 16.22. Found: C, 40.80; H, 3.35; N, 16.14%. ESI MS: (m/z) 1049.53 [MH^+]. Calcd av. m/z 1049.10. Selected IR (KBr, cm^{-1}) 1645 s [ν(C=N)]; 1541 s [ν(C–O)]; 1339 [$\nu(NO_3^-$] 1090 s [$\nu(ClO_4)$]; 625 m [ν(M-O]; Λm (DMF, 298 K): 139 S cm^2 mol^{-1}.

3. Results and discussion

The cryptates [GdML(NO_3)]$^+$ (ClO_4) [M = VO(IV), Co(II), Ni(II), Cu(II)] were synthesized by a 2-step process: (1) the mononuclear cryptate precursors [Gd(HL)(NO_3)].2H_2O, were synthesized and the hetero binuclear cryptates were formed by the reaction of the precursors with [M = VO(IV), Co(II), Ni(II), Cu(II)] ions. Because the Gd(III) ions in the cryptates were kinetically inert and thermodynamically stable while the encapsulated water molecule was labile, a second metal ion [M = VO(IV), Co(II), Ni(II), Cu(II)] replaces the water molecule during the reaction process. The added base removed the protons of the phenolic groups in the precursor. Due to the flexibility of the cryptand it was able to adjust its cavity to match the differently sized metal ions.

3.1. Spectral studies

The values of molar conductivity of the 4 binuclear complexes are located in the range of 1:2 electrolytes (132–139 S cm^2 mol^{-1}) in DMF.[23] The FTIR spectrum of each complex showed an intense band at 1645 cm^{-1} attributable to ν(C=N), which was different from the split bands of the mononuclear cryptates due to the unsymmetrical coordination of gadolinium(III) ion to imine nitrogen atoms. The bands at 1478 and 1281 cm^{-1} were due to ν (N=O) (ν_1) and ν_{asym} (NO_3^-) vibration (ν_5) of coordinated nitrates. The ν_{asym} (NO_3^-) vibration (ν_2) at 1078 cm^{-1} was characteristic of a bidentate nitrate group.[24,25] The strong sharp band at 1367 cm^{-1} was characteristic of ionic nitrate.[26] The IR spectrum shows that there are only coordinated nitrates in the complex. The bands at 1070 and 645 cm^{-1} were characteristic of ClO_4^- ion.

3.2. ESI mass spectral analysis

The ESI mass spectra of mono and binuclear complexes [GdLH(NO_3], [GdVOL(NO_3)]$^+$, and [GdCuL(NO_3)]$^+$ show the molecular ion peak (M^+) at m/z = 988.20, 1054.40, and 1049.53, respectively. The spectra show some prominent peaks corresponding to various fragments of the complexes. The ESI mass spectra of the complexes [GdLH(NO_3], [GdVOL(NO_3)]$^+$, and [GdCuL (NO_3)]$^+$ are shown in Figures 1a–c.

3.3. Electronic spectra

The UV-Vis spectra of these cryptates were dominated by intense ligand bands at ca. 275, 286, and 380 nm. The band at 394 nm was assigned to the C=N chromophores, while the other 2 bands were designated as a π–π^* transition of the K band of the benzene rings. The data are given in Table 1. The d–d transition of M [VO(IV), Co(II), Ni(II) and Cu(II)] in cryptates is at about 610–925 nm, showing that all d metal ions were located in an octahedral coordination environment. The spectra are given in Figures 2a and b.

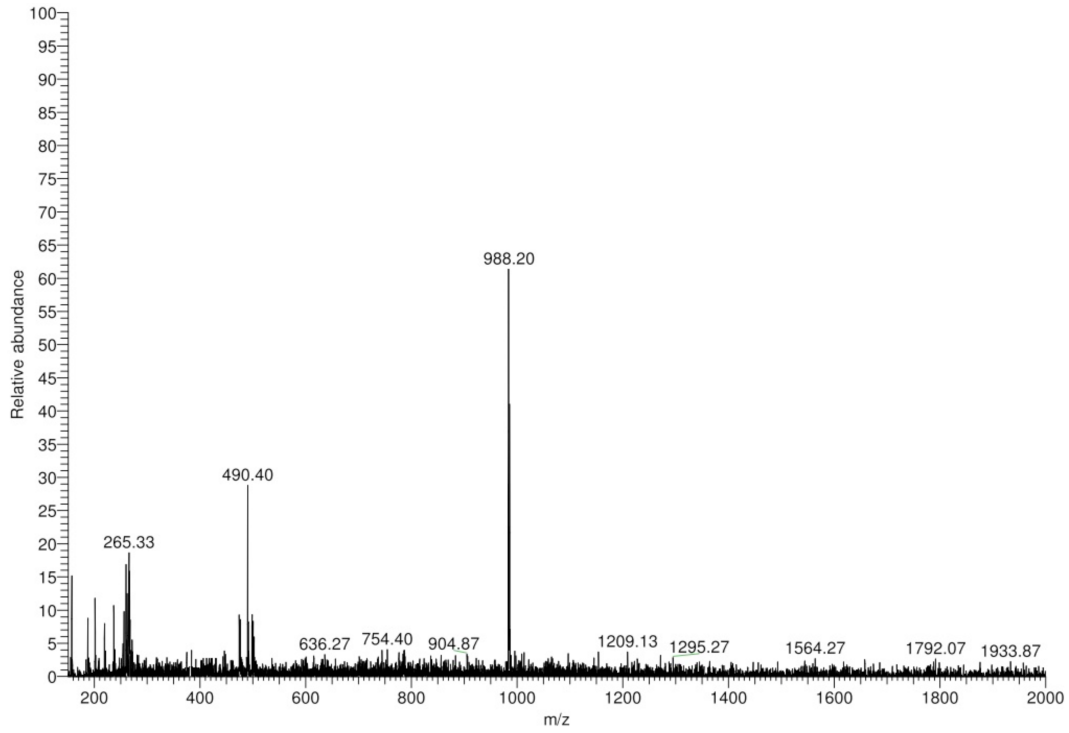

Figure 1. (a) ESI mass spectrum of [GdLH(NO_3)] complex m/z 988.20 [MH^+].

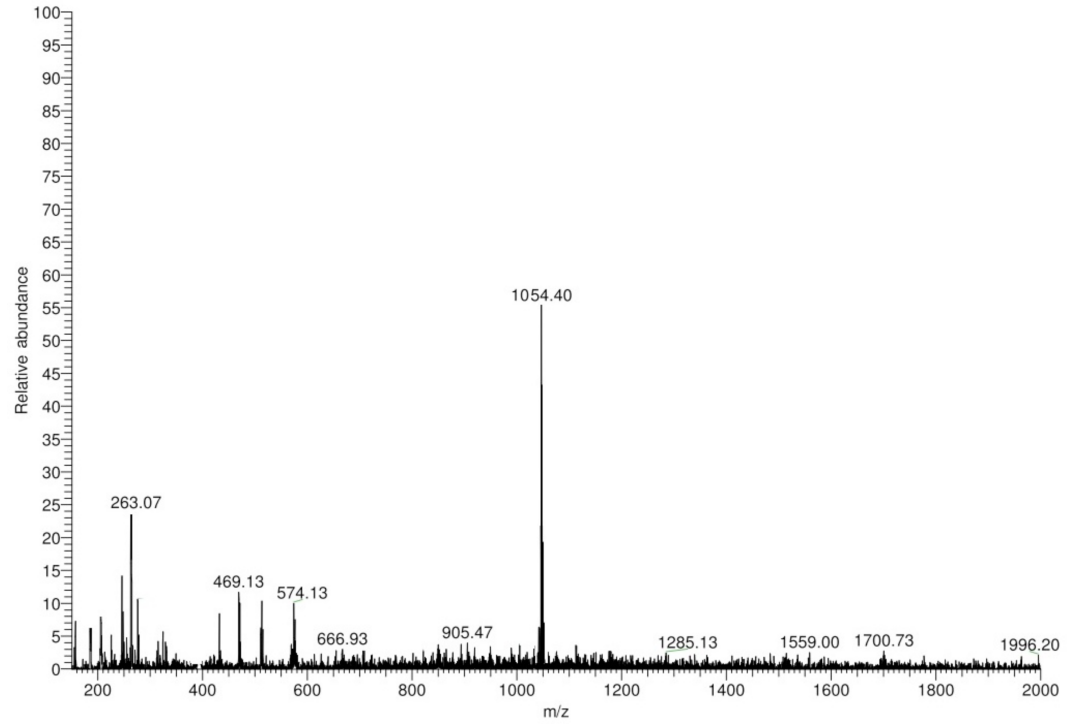

Figure 1. (b) ESI mass spectrum of $[GdVOL(NO_3)]^+$ complex m/z 1054.40 [MH^+].

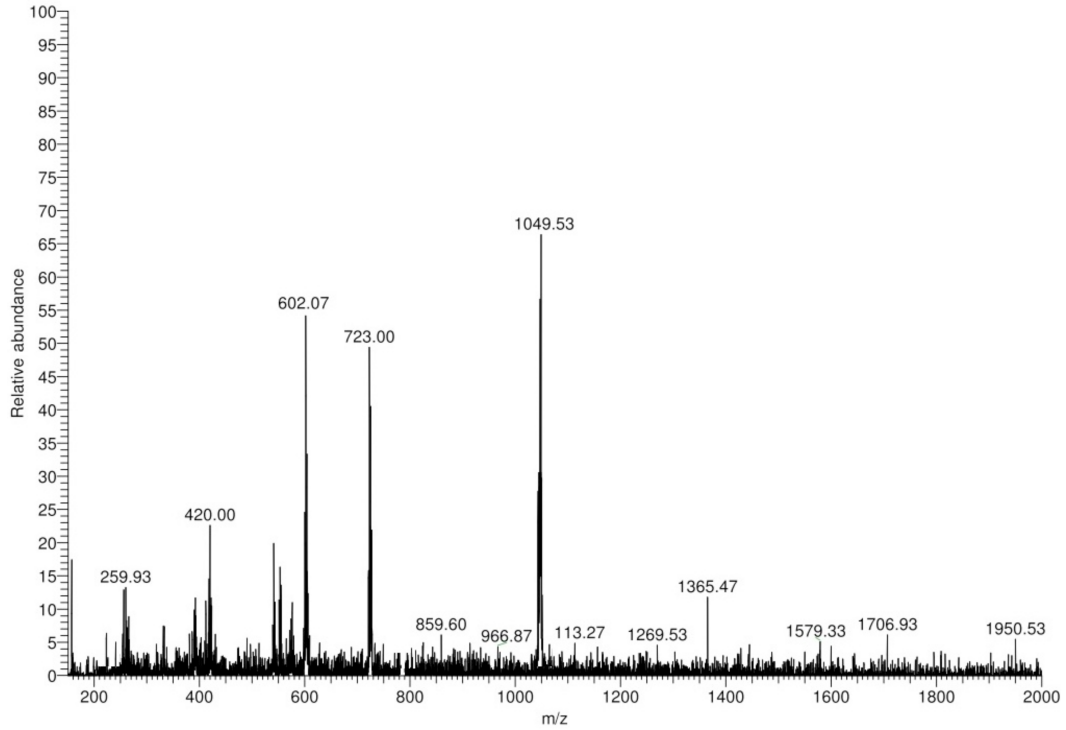

Figure 1. (c) ESI mass spectrum of $[GdCuL(NO_3)]^+$ complex m/z 1049.53 $[MH^+]$.

Table 1. Electronic spectral data of $[Gd(III)ML(NO_3)]^+$ M = VO(IV), Co(II), Ni(II), Cu(II) complexes.

Sl. no.	Complexes	λ_{max} (nm) (ε/M^{-1} cm^{-1})	
		d–d	Charge transfer
1	$[GdLH(NO_3)]$		380(16,189) 320 (20,642) 275(23,876)
2	$[GdVOL(NO_3)]^+$	823(3385)	388(16,089) 283 (22,608)
3	$[GdCoL(NO_3)]^+$	925(1394)	394(15,955) 286 (22,564)
4	$[GdNiL(NO_3)]^+$	740(4191)	408(15,841) 289 (22,497)
5	$[GdCuL(NO_3)]^+$	610(7887)	418(15,721) 293 (22,372)

3.4. Luminescence studies of cryptates [1–5]

Emission spectra of cryptates [**1**–**5**] in DMF solution with excitation at 400 nm are shown in Figure 3. Compared with the mononuclear gadolinium(III) cryptate **1**, cryptates **4** and **5** $\{[GdNiL(NO_3)]^+$ and $[GdCuL(NO_3)]^+\}$ show lower intensity of emission band in the range 420–650 nm, indicating that the fluorescence of Gd(III) ion in the cavity was quenched by the encapsulated Cu(II) and Ni(II) ions. However, the characteristic emission spectrum of Gd(III) ion for cryptate **2** and **3** $\{[GdVOL(NO_3)]^+$ and $[GdCoL(NO_3)]^+\}$ was observed. All emissions arise from the ^6D_j level corresponding to the $^5D_0 \rightarrow {}^8S_{7/2}$ (ΔJ = 0, 1–4) transition. The weak band at 450 nm arises from the $^5D_0 \rightarrow {}^8S_{7/2}$ transition. The band around 470 nm for $^5D_0 \rightarrow {}^8S_{7/2}$, which was magnetic-dipole allowed, was hardly affected by a change in the coordination environment. The intense band around 675 nm for $^5D_0 \rightarrow {}^8S_{7/2}$ was an electric-dipole allowed transition and its emission intensity was sensitive to the coordination environment of Gd(III). This shows that fluorescence emission of Gd(III) ions in the cryptates was influenced by the encapsulated transition metal ions.

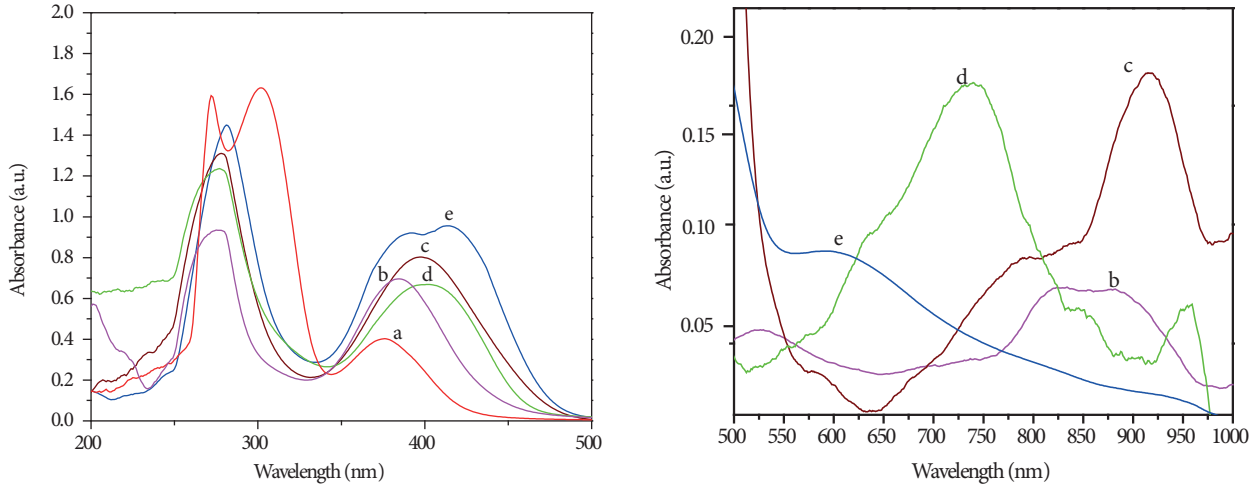

Figure 2. (a) Electronic spectra of a) [GdLH(NO$_3$)], b) [GdVOL(NO$_3$)]$^+$, c) [GdCoL(NO$_3$)]$^+$, d) [GdNiL(NO$_3$)]$^+$, and e) [GdCuL(NO$_3$)]$^+$ complexes. (b) Electronic spectra of b) [GdVOL(NO$_3$)]$^+$, c) [GdCoL(NO$_3$)]$^+$, d) [GdNiL(NO$_3$)]$^+$, and e) [GdCuL(NO$_3$)]$^+$ complexes.

3.5. Lifetime measurement of cryptates [1–5]

Advances in the design and miniaturization of the lasers and electronics required for time-correlated single photon counting (TCSPC) measurement of fluorescence lifetime have simplified the use of the time domain method. This fitting clearly shows that the lifetime decay profile of the complexes was well fitted with tri exponential and bi exponential fitting. The emission spectra and decay time measurements for the [Gd(III)M] M = VO(IV), Co(II), Ni(II), Cu(II) cryptates allowed the identification of the highest ligand triplet state shown in Figure 4. [GdCoL(NO$_3$)]$^+$ cryptate had a higher lifetime value compared to the other cryptates. The order of the excited state lifetime was as follows:

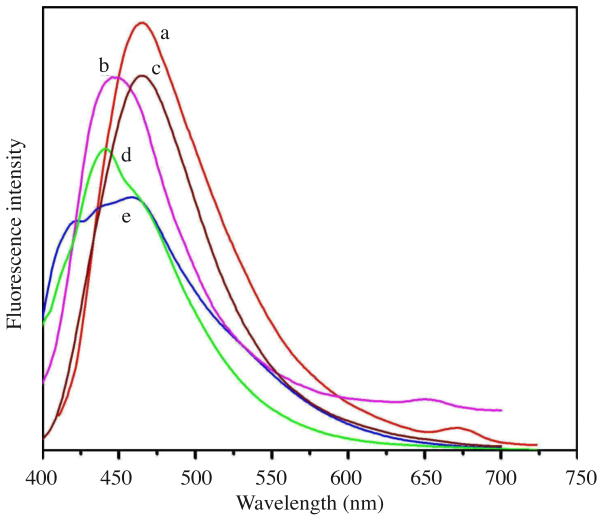

Figure 3. Luminescent studies of (a) [GdLH(NO$_3$)], (b) [GdVOL(NO$_3$)]$^+$, (c) [GdCoL(NO$_3$)]$^+$, (d) [GdNiL(NO$_3$)]$^+$, and (e) [GdCuL(NO$_3$)]$^+$ complexes.

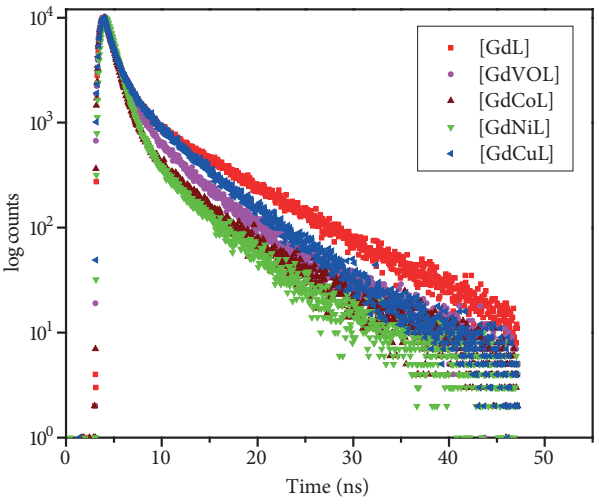

Figure 4. Lifetime measurement for (a) [GdLH(NO$_3$)], (b) [GdVOL(NO$_3$)]$^+$, (c) [GdCoL(NO$_3$)]$^+$, (d) [GdNiL(NO$_3$)]$^+$, and (e) [GdCuL(NO$_3$)]$^+$ complexes.

$[GdLH(NO_3)] < [GdCuL(NO_3)]^+ < [GdNiL(NO_3)]^+ < [GdVOL(NO_3)]^+ < [GdCoL(NO_3)]^+$.

The lifetime decay curve for $[GdNiL(NO_3)]^+$ was only bi exponential, whereas the other 4 cryptates {$[GdLH(NO_3)]$, $[GdVO(NO_3)]^+$, $[GdCoL(NO_3)]^+$, and $[GdCuL(NO_3)]^+$} were tri exponential. The data are given in Table 2. The exponential decay behavior depends on the number of different luminescent centers, energy transfer, defects, and impurities in the host.

Table 2. Lifetime measurement of $[Gd(III)ML(NO_3)]^+$ M = VO(IV), Co(II), Ni(II), Cu(II) complexes.

Complexes	τ_1/ns	α_1 (%)	τ_2/ns	α_2 (%)	τ_3/ns	α_3 (%)	χ^2
$[GdLH(NO_3)]$	0.14	10.22	1.32	39.28	8.10	50.50	1.03
$[GdVOL(NO_3)]^+$	0.04	20.50	1.15	42.02	5.37	37.48	1.13
$[GdCoL(NO_3)]^+$	0.10	5.19	1.00	64.18	5.26	30.63	1.13
$[GdNiL(NO_3)]^+$	—	—	1.05	72.87	4.96	27.13	1.09
$[GdCuL(NO_3)]^+$	0.50	14.48	1.36	34.45	5.84	51.08	1.08

3.6. Cyclic voltammetric behavior of complexes [1–5]

The cyclic voltammogram of mononuclear complex $[Gd(H_3L)(NO_3)].2H_2O$ in DMF in the range 0.0 to –2.50 V at the scan rate of 0.05 V s^{-1} is given in Figure 5, which shows well-defined cathodic peak potential of E_{pc} = –1.95 V (Ag/AgCl). The ratio of the anodic to cathodic peak currents i_{pa}/i_{pc} was close to unity at low scan rates. Cryptate **5** $[Gd(III)Cu(II)L]^+$ complex shows 2 well-defined cathodic peak potentials of E^1_{pc} = –1.10 V, E^2_{pc} = –1.80 V (Ag/AgCl). The first reduction process was Cu(II)/Cu(I). The second reduction process was observed at the cathodic potentials E^2_{pc} –1.80 V, which may be corresponding to the mono nuclear cryptate [Gd(III)LH] peak potential, which was ligand-centered. The overall electrode reaction was suggested to be LGd(III)Cu(II) → LGd(III)Cu(I) → $L^\bullet$ Gd(III)Cu(I). The electrochemical data for all the complexes are given in Table 3. Cryptate **2** $[GdVOL(NO_3)]^+$ shows 2 well-defined cathodic peaks: E^1_{pc} = –1.65 V and E^2_{pc} = −2.20 V. The first reduction peak was assigned to Gd(III)VO(IV) → Gd(III)VO(III) and the second redox process, observed at –2.20 V, was assigned to LGd(III)VO(III) →$L^\bullet$ Gd(III)VO(III), and anodic peaks were observed at E_{pa} = 0.50 V. The cyclic voltammogram for the electrochemical oxidation reaction is shown in Figure 6. The electrochemical oxidation process was due to Gd(III)VO(IV) → Gd(III)VO(V). Cryptate **3** $[GdCoL(NO_3)]^+$ shows 2 well-defined peaks at E^1_{pc} = –1.30 V and E^2_{pc} = –1.900 V in the cathodic direction and an anodic peak was also observed at E_{pa} = 0.54 V. The first reduction peak was assigned to Gd(III)Co(II) → Gd(III)Co(I) and the second to LGd(III)Co(I)→ $L^\bullet$ Gd(III)Co(I). The electrochemical oxidation reaction was Gd(III)Co(II) → Gd(III)Co(III). Cryptate **4** $[GdNiL(NO_3)]^+$ shows 2 well-defined peaks in the cathodic direction E^1_{pc} = –1.15 V and E^2_{pc} = –1.85 V, and an anodic peak was observed at E_{pa} = 0.62 V. The first reduction peak was assigned to Gd(III)Ni(II) → Gd(III)Ni(I) and the second redox process was assigned to LGd(III)Ni(I) → $L^\bullet$ Gd(III)Ni(I). The oxidation reaction was Gd(III)Ni(II)/Gd(III)Ni(III). The electrochemical data for cryptates **1–5** are listed in Table 3. They show that the reduction potential of Gd(III) binuclear complexes shifted to a less negative potential compared to mononuclear Gd(III) complex, influenced by the d metal ions VO(IV),Co(II), Ni(II), and Cu(II) encapsulated in the cryptate. The sequence of influence of metals ions is Cu(II) > Ni(II) > Co(II) > VO(IV).

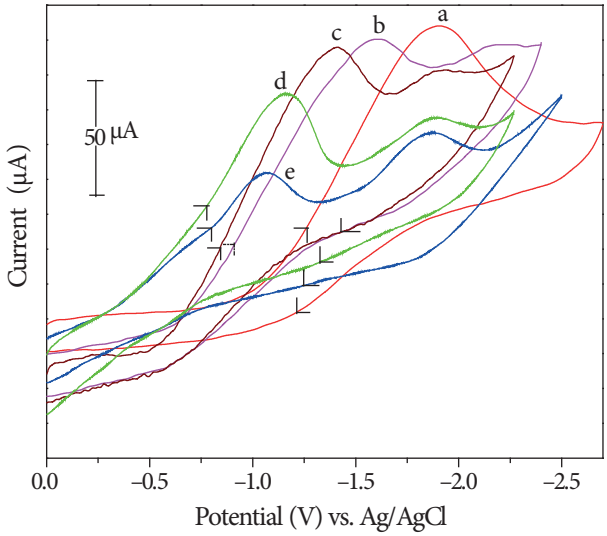

Figure 5. Cyclic voltammograms of mono and binuclear complexes reduction at cathodic potential (a) $[GdLH(NO_3)]$,(b) $[GdVOL(NO_3)]^+$, (c) $[GdCoL(NO_3)]^+$, (d) $GdNiL(NO_3)]^+$, and (e) $[GdCuL(NO_3)]^+$. [Complex] = 1.05×10^{-3} mol dm^{-3}, [TABP] = 0.1 mol dm^{-3}, scan rate = 0.050 V s^{-1}.

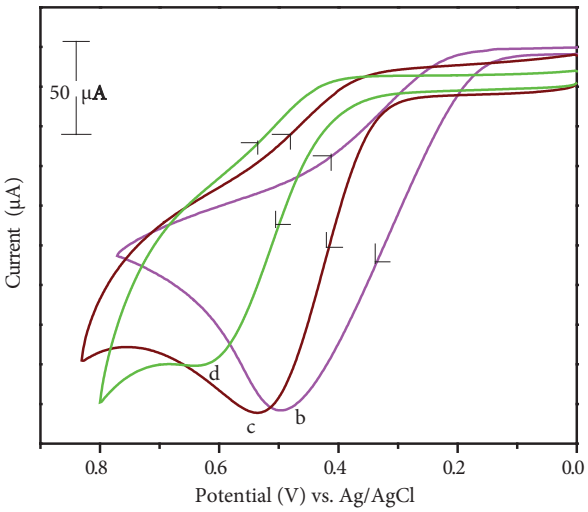

Figure 6. Oxidation process at anodic potential of binuclear complexes (b) $[GdVOL(NO_3)]^+$, (c) $[GdCoL(NO_3)]^+$, and (d) $[GdNiL(NO_3)]^+$ [complex] = 1.05×10^{-3} mol dm^{-3}, [TABP] = 0.1 mol dm^{-3}, scan rate = 0.050 V s^{-1}.

Table 3. The reduction and oxidation potential values(V) vs. Ag/AgCl of $[Gd(III)ML(NO_3)]^+$ [M = VO(IV), Co(II), Ni(II), Cu(II)] cryptates in DMF.

Complexes	Reduction potential E^1_{pc}/V	(cathodic) E^2_{pc}/V	Oxidation (anodic) potential E^1_{pa}/V
$[GdLH(NO_3)]$	–1.95	–	-
$[GdVOL(NO_3)]^+$	–1.65	–2.20	0.50
$[GdCoL(NO_3)]^+$	–1.30	–1.90	0.54
$[GdNiL(NO_3)]^+$	–1.15	–1.85	0.62
$[GdCuL(NO_3)]^+$	–1.10	–1.80	-

Measured by CV at 0.050 V s^{-1} scan rate. E vs. Ag/AgCl conditions: GC working electrode and Ag/AgCl reference electrodes; supporting electrolyte TBAP; concentration of complex 1×10^{-3} M, concentration of TBAP 1×10^{-1} M.

3.7. Magnetic behavior

3.7.1. Magnetic properties of $[GdCuL(NO_3)]^+$ complex

Owing to the difficulties in analyzing the magnetic properties of (Ln, Cu) pairs involving a Ln^{3+} ion, which possesses a disorder orbital moment,[27] the temperature (T) dependence of magnetic susceptibility (χ_m) in the range 2.0–300 K is shown in Figure 7. The effective magnetic moment (μ_{eff}) at 300 K is 7.90 μ_B, which was slightly greater than the spin-only value (8.10 μ_B) calculated by $\mu^2_{eff} = \mu^2_{Cu} + \mu_{Gd}{}^2$, by assuming that there was no magnetic interaction between Cu(II) ($S_{Cu} = 1/2$) and Gd(III) ($S_{Gd} = 7/2$). When the

temperature decreased, the μ_{eff} increased slowly from 7.95 μ_B at 50 K and then increased steeply to the maximum value (9.75 μ_B) at 0.50 K. The maximum value was longer than the spin-only value (8.94 μ_B) for spin state $S = 4$, which arises from ferromagnetic spin-coupling of the present spin system ($S_{Cu} = 1/2$, $S_{Gd} = 7/2$). Therefore, the observed magnetic behavior clearly demonstrates intermolecular ferromagnetic spin-coupling between Cu(II) and Gd(III) and, possibly, an intermolecular antiferromagnetic coupling interaction in the cryptate. The magnetic data were analyzed on the basis of the spin-only equation derived from a spin Hamiltonian $H = -JS_{Cu}S_{Gd}$; χ_m was expressed as follows:

$$\chi_m = \frac{4Ng^2\beta^2}{kT}\left[\frac{15 + 7\exp(-8J/kT)}{9 + 7\exp(-8J/kT)}\right] \quad (1)$$

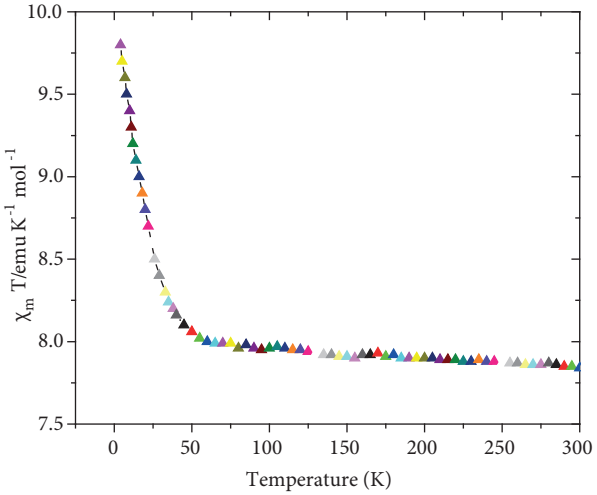

Figure 7. Thermal dependence of $\chi_M T$ for $[GdCuL(NO_3)]^+$ at 0.5 T. The full line corresponds to the best data fit.

On fitting Eq. (1), the parameters $g = 1.97$ and $J = -0.66$ cm^{-1} were obtained with an agreement factor $R = 6.40 \times 10^{-4}$ [$R = \Sigma(\chi_{obs}T. \ \chi_{calc}T)^2/\Sigma(\chi_{obs}T)^2$; χ_{calc} and χ_{obs} denote the calculated and observed molar magnetic susceptibilities, respectively]. There was no doubt that the observed ferromagnetic behavior was an intrinsic property of the core. The J values are slightly lower for GdO_3Cu than those previously published for 4 structurally characterized heterodinuclear (Gd, Cu) complexes.[28] The structural study of the complex shows that a third bridge joins an axial site of Gd to an axial site of Cu, which has, at best, a very feeble spin density. The observed J value (4.2 cm^{-1}) is quite similar to those found for complexes in which the magnetic interaction was mediated by a double bridge, GdO_3Cu, as in previous examples. Furthermore, the very good fit obtained for Figure 7 with the help of the above expression corresponding to a dinuclear Gd-Cu complex confirms the dinuclear character of the powdered sample.

3.8. Dye-sensitized solar cell studies

The as-prepared gadolinium complexes were utilized as dye molecules in the fabrication of DSSCs and their performance is summarized in Table 4 (Figure 8). Anchoring of gadolinium complexes on the TiO_2 surface may occur via –OH and $–NO_2$ group of ligands. All the gadolinium complexes showed moderate conversion efficiency compared to that of standard N3 dye under identical conditions (see Table 4; inset of Figure 8). The order of efficiency observed for the complexes studied in this work correlates roughly well with the absorption cut-off

wavelengths observed for the complexes. That is, $[GdNiL(NO_3)]^+$ complex shows high cut-off wavelength (l > 470 nm) and greater efficiency compared to the other complexes.

Table 4. Performance parameters of dye-sensitized solar cells constructed by using the Gd metal based dyes under the illumination of 40 mW cm^{-2}.

S. no.	Dyes	Jsc (mA cm^{-2})	Voc (mV)	Fill factor (FF)	Efficiency (%)
1	$[GdLH(NO_3)]$	0.757	393	0.4311	0.32
2	$[GdVOL(NO_3)]^+$	0.222	435	0.4083	0.10
3	$[GdCoL(NO_3)]^+$	0.459	424	0.3714	0.18
4	$[GdNiL(NO_3)]^+$	0.609	587	0.4299	0.38
5	$[GdCuL(NO_3)]^+$	0.370	602	0.5179	0.29
6	N3	6.543	748	0.4601	5.63

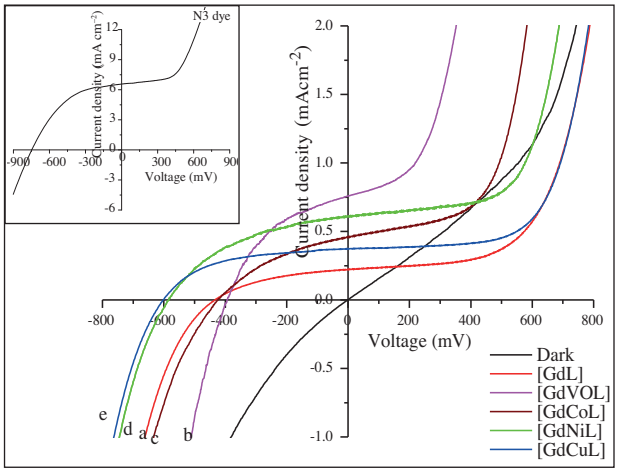

Figure 8. Photocurrent density–voltage (J–V) curves of DSSCs based on the Gd(III) metal based dyes under the illumination of 40 mW cm^{-2}. a) $[GdLH(NO_3)]$, (b) $[GdVOL(NO_3)]^+$, (c) $[GdCoL(NO_3)]^+$, (d) $GdNiL(NO_3)]^+$, and (e) $[GdCuL(NO_3)]^+$; the inset figure shows the J–V curve of standard N3 curve.

Mono and hetero binuclear cryptates $[GdML]^+$ [M = VO(IV), Co(II), Ni(II), Cu(II)] were synthesized by a 2-step method. Variable temperature magnetic susceptibility of $[GdCuL(NO_3)]^+$ confirms the occurrence of an overall intermolecular ferromagnetic interaction. The lifetime decay curve for $[GdNiL(NO_3)]^+$ was only bi exponential, with $[GdCoL(NO_3)]^+$ cryptate having a high lifetime value. The cyclic voltammogram of each cryptate showed a pair of well-defined redox peaks and an irreversible cathodic peak assigned to the stepwise reduction of M [VO(IV), Co(II), Ni(II), Cu(II)]. The reduction potential shifted more negatively and oxidation potential shifted to a more positive potential compared to free M^{2+} ion and were influenced by lanthanide ions in the cryptates. The degree of negative shift followed the order $[GdCuL(NO_3)]^+ > [GdNiL(NO_3)]^+ > [GdCoL(NO_3)]^+ > [GdVOL(NO_3)]^+ >$ [GdLH]. DSSC efficiency was in the following order: [GdLH] $< [GdVOL(NO_3)]^+ < [GdCoL(NO_3)]^+ < [GdNiL(NO_3)]^+ < [GdCuL(NO_3)]^+$.

4. Acknowledgments

Financial support from the CSIR New Delhi is gratefully acknowledged. The authors also acknowledge the National Centre for Ultrafast Process, University of Madras, for the lifetime measurements.

References

1. Regan, B.; Gratzel, M. *Nature* **1991**, *353*, 737–740.
2. Hagfeldt, A.; Gratzel, M. *Acc. Chem. Res.* **2000**, *33*, 269–277.
3. Gratzel, M. *Nature* **2000**, 414, 1338–1341.
4. Gratzel, M. *Nature* **2003**, *421*, 586–587.
5. Moreira Goncalves, L.; Bermudez, V.; Aguilar Ribeiro, H.; Magalhaes Mendes, A. *Energy Environ. Sci.* **2008**, *1*, 655–667.
6. (a) Ma, X.; Hua, J.; Wu, W.; Jin, Y.; Meng, F.; Zhan, W.; Tian, H. *Tetrahedron* **2008**, *64*, 345–350; (b) Cao, Y.; Bai, Y.; Yu, Q.; Chang, Y.; Liu, S.; Shi, D.; Gao, F.; Wang, P. *J. Phys. Chem.* **2009**, *113*, 6290–6297.
7. Zhou, G.; Pschirer, N.; Schoneboom, J. C.; Eickemeyer, F.; Baumgarten, M.; Mullen, K. *Chem. Mater.* **2008**, *20*, 1808–1815.
8. Alexander, V. *Chem. Rev.* **1995**, *95*, 273–342.
9. Evans, C. H. *Biochemistry of Lanthanide,* Plenum, New York, 1990.
10. Parkers, D.; Williams, J. A. G. *J. Chem. Soc. Dalton Trans.* **1996**, 3613–3628.
11. Sabbatini, N.; Guardigli, M. *Coord. Chem. Rev.* **1993**, *123*, 201–228.
12. (a) Zanello, P.; Tamburini, S.; Vigato, P. A.; Mazzocchin, G. A. *Coord. Chem. Rev.* **1987**, *77*, 165–273; (b) Bosnich, B. *Inorg. Chem.* **1999**, *38*, 2554–2562; (c) Costes, J. P.; Dupuis, A.; Laurent, J. P. *J. Chem. Soc., Dalton Trans.* **1998**, 735–736.
13. Drew, M. G. B.; Howarth, O. W.; Harding, C. J.; Martin, N.; Nelson, J. *J. Chem. Soc. Chem. Commun.* **1995**, 903–904.
14. Avecilla, F.; De Bias, A.; Bastida, R.; Fenton, D. E.; Mahia, J.; Macias, A.; Plates, C.; Rodriguez, A.; Rodriguez-Blas, T. *Chem. Commun.* **1999**, 125–126.
15. Feng, C. J.; Luo, Q. H.; Duan, C. Y.; Shen, M. C.; Liu, Y. J. *J. Chem. Soc. Dalton Trans.* **1998**, 1377–1380.
16. Chen, Q. Y.; Luo, Q. H.; Wang, Z. L.; Chen, J. T. *Chem. Commun.* **2000**, 1033–1034.
17. (a) Xu, Z. Q.; Pead, P. W.; Hibbs, D. E.; Hursthouse, M. B.; Malik, K. M. A.; Retting, B. O.; Seid, M.; Summers, D. A.; Pink, M.; Thompson, R. C.; Orvig, C. *Inorg. Chem.* **2000**, *39*, 508–516. (b) Brechin, E. K.; Harris, S. G.; Parsons, S.; Winpenny, P. E. P. *J. Chem. Soc. Dalton Trans.* **1997**, 1665–1671.
18. (a) Costes, J. P. Dahan, F.; Dupuis, A. *Inorg. Chem.* **2000**, *39*, 165–168; (b) Piguet, C.; Edder, C.; Rigault, S.; Bernardinelli, G.; Bunzli, J. C. G.; Hopfgartner, G. *J. Chem. Soc. Dalton Trans.* **2000**, 3999–4006.
19. Chen, Q. Y.; Luo, Q. H.; Zheng, L. M.; Wang, Z. L.; Chen, J. T. *Inorg. Chem.* **2002**, *41*, 605–609.
20. Bencini, A.; Gatteschi, D. *EPR of Exchange Couples Systems,* Springer-Verlag, Berlin, 1990.
21. Sirimanne, P. M.; Jeranko, T.; Bogdanoff, P.; Fiechter, S.; Tributsch, H. *Semicond. Sci. Technol.* **2003**, *18*, 708–712.
22. Nogueira, A. F.; Durrant, J. R.; De Paoli, M. A. *Adv. Mater.* **2001**, *13*, 826–830.
23. Geary, W. J. *Coord. Chem. Rev.* **1971**, *7*, 81–122.
24. K. Nakamoto, *Infrared and Raman Spectra of Inorganic and Coordination Compounds,* Wiley-Interscience, New York, 3rd edn. 1978.
25. Suresh Kumar, D.; Alexander, V. *Inorg. Chim. Acta* **1995**, *238*, 63–71.
26. Carnall, W. T.; Siegel, S.; Ferraro, J. R.; Tani, B.; Gebert, E. *Inorg. Chem.* **1973**, *12*, 560–564.
27. Taniguchi, S. *Bull. Chem. Soc. Jpn.* **1984**, *57*, 2678–2683.
28. Costes, J. P.; Dahan, F.; Dupuis, A.; Laurent, J. P. *New J. Chem.* **1998**, 1525–1529.